Elucidating Charge Separation Dynamics in a Hybrid Metal-Organic Framework Photocatalyst for Light-Driven H_2 Evolution

Sizhuo Yang,[a] *Donghua Fan,*[b] *Wenhui Hu,*[a] *Brian Pattengale,*[a] *Cunming Liu,*[c] *Xiaoyi Zhang,*[c] *Jier Huang*[a]*

[a]Department of Chemistry, Marquette University, Milwaukee, Wisconsin, 53201

[b]School of Applied Physics and Materials, Wuyi University, Jiangmen, 529020, China

[c]X-ray Science Division, Argonne National Laboratory, Argonne, Illinois, 60349

Corresponding Author

Jier Huang (jier.huang@marquette.edu)

ABSTRACT. Metal-organic frameworks (MOFs) have emerged as novel scaffolds for artificial photosynthesis due to their unique capability in incorporating homogeneous photosensitizer and catalyst to their robust heterogeneous matrix. In this work, we report the charge separation dynamics between molecular Ru-photosensitizer and Pt-catalyst, both of which were successfully incorporated into a Zr-MOF that demonstrates excellent activity and stability for light-driven H_2 generation from water. Using optical transient absorption (OTA) spectroscopy, we show that charge separation in this hybrid MOF occurs via electron transfer (ET) from Ru-photosensitizer to Pt-catalyst. Using Pt L_3-edge X-ray transient absorption (XTA) spectroscopy, we observed the intermediate reduced Pt site, directly confirming the formation of charge separated state due to ET from Ru-photosensitizer and unravelling their key roles in photocatalysis.

Introduction.

The utilization of solar energy to drive hydrogen generation from water is one of the best solutions to address the global energy and environmental problems.[1-2] In the past decades, diverse photocatalytic systems for H_2 generation including homogeneous and semiconductor based/metal doped heterogenous systems have been developed, which typically consist of light harvesting materials, catalysts, and proton and electron sources.[3-6] However, the performance of these systems for H_2 generation in terms of both activity and stability is far from satisfactory. In addition to poor stability and efficiency, the homogenous molecular systems suffer from the difficulty in recycling from the reaction system.[7-10] While heterogeneous systems have shown potential in long-term stability and high activity, these materials suffer from two major limitations that hamper their further use as photocatalytic materials: 1) the lack of design flexibility, and 2) the poor understanding of the catalytic active species.[11-15]

To integrate the beneficial features and overcome the drawbacks of homogeneous and heterogeneous photocatalytic systems for H_2 generation, metal organic frameworks (MOFs), an emerging class of porous crystalline materials, could be a judicious choice. MOFs are constructed from metal ions/clusters covalently interconnected to multidentate organic linkers.[16-23] The versatility of these components not only offers the capability to tune their cavity but also allows incorporation of molecular functional units into its heterogeneous crystal matrix, opening up the possibility to address the stability issues and allow high resolution studies of the incorporated catalytic active sites using a suite of physical characterization methods.[24-31]

Due to these reasons, recent efforts on MOF photocatalysis have extended to incorporate molecular photosensitizers or/and catalysts into MOFs structure. While a large number of functionalized MOF systems with either molecular photosensitizers (PSs) or catalysts incorporated

into the framework have been reported recently toward versatile applications,[24-27, 32-49] there are only two examples that integrate both PS and catalysts for photocatalytic H_2 generation. One example includes the incorporation of $[Ru(dcbpy)(bpy)_2]^{2+}$ (dcbpy=2,2'bipyridyl-5,5'-dicarboxylic acid) and $Pt(dcbpy)Cl_2$ complex to the MOFs scaffold (UIO-67), which can serve as PSs and catalysts, respectively, for photocatalytic H_2 generation from water.[40] The second example reported the successful incorporation of Ir(III) complex as PS and Pt(II) complex as catalyst into UIO-67 MOFs, which demonstrated significant increase in both H_2 evolution activity and robustness compared to its homogenous counterpart.[50] While these examples demonstrate the potential of MOFs as versatile platform for incorporating molecular modules necessary for photocatalytic applications, the fundamental aspects with regard to light harvesting and charge separation (CS) dynamics of these molecular functional units in MOFs remain less explored,[19, 37-38, 47, 51-55] yet it is essential for further development of these materials. Herein, we report the CS dynamics in $[Ru(dcbpy)(bpy)_2]^{2+}$ and $Pt(dcbpy)Cl_2$ functionalized UIO-67 MOF (Ru-Pt-UIO-67, Figure 1a) which demonstrates efficient H_2 generation from water using the combination of optical transient absorption (OTA) and X-ray transient absorption (XTA) spectroscopy. The direct correlation of the fundamental insights into the CS dynamics with their function for photocatalysis provides important guidance in rational design of new and efficient photocatalytic MOF systems.

Experimental Section.

Materials. $ZrCl_4$ (> 99.5%, Strem Chemicals), 2,2-bipyridine-5,5-dicarboxylic acid (H_2bpdcy) (97%, Ark Pharm), 2, 2-dipyridyl (>99%, Acros Organics), 4,4-biphenyldicarboxylic acid (bpdc) (98%, Acros Organics), glacial acetic acid (regent ACS, Acros Organics). $Ru(bpy)_2Cl_2$[56] and $Pt(dcbpy)Cl_2$[57] were synthesized according to previous literature.

), 8.13 (d, 2 H), 8.06 (m, 4 H), 7.75 (d, 4 H) and 7.42 (m, 4 H).

Synthesis of Ru-UIO-67, Ru-Pt-UIO-67 and Pt-UIO-67. The synthesis of these MOFs follow the previous reported procedure for UIO-67 type MOF with slightly modification.[43, 58]

Ru-Pt-UIO-67: $ZrCl_4$ (30.0 mg, 0.13 mmol), 4,4-biphenyldicarboxylic acid (bpdc) (24.0 mg, 0.1 mmol), Rudcbpy (10.0 mg, 0.015 mmol), $Pt(dcbpy)Cl_2$ (6.0 mg, 0.012 mmol) and glacial acetic acid (250 μL, 4.3 mmol) were dispersed in DMF (5 mL), and then transferred to autoclave, the sample was sonicated for 20 mins and placed in an oven. The temperature was set at 120 °C for 24 hours. After cooling down to room temperature, the resulting solid was isolated by centrifugation, and was washed with methanol repeatedly before being dried under vacuum. Yield: 58mg (83%). The Ru and Pt content in MOF is determined by atomic absorption spectroscopy to be 1.2 wt% and 2 wt%.

Ru-UIO-67: $ZrCl_4$ (30.0 mg, 0.13 mmol), 4,4-biphenyldicarboxylic acid (bpdc) (29.0 mg, 0.12 mmol), Rudcbpy (10.0 mg, 0.015 mmol), and glacial acetic acid (250 μL, 4.3 mmol) were dispersed in DMF (5 mL), the same synthetic procedure as Ru-Pt-UIO-67 was then used. Yield: 60 mg (86.9%).

Pt-UIO-67: $ZrCl_4$ (30.0 mg, 0.13 mmol), 4,4-biphenyldicarboxylic acid (bpdc) (29.0 mg, 0.12 mmol), $Pt(dcbpy)Cl_2$ (6.0mg, 0.012mmol), and glacial acetic acid (250 μL, 4.3 mmol) were dispersed in DMF (5 mL), the same synthetic procedure as Ru-Pt-UIO-67 was used. Yield: 55mg (84.6%).

Characterization and General procedure. UV-Visible absorption spectra were taken using an Agilent 8453 spectrometer. PXRD data were collected by using Rigaku Miniflex II XRD diffractometer with Cu Kα radiation. ^1H NMR spectra were collected at room temperature with a

Varian 400 MHz spectrometer. Gas adsorption isotherms were performed by using the surface area analyzer ASAP-2020. N_2 gas adsorption isotherms were measured at 77K using a liquid N_2 bath. The amount of H_2 generated was quantified using Agilent 490 micro gas chromatograph (5 Å molecular sieve column). To make hybrid MOF films, 1 mg MOF was mixed with 0.5 mL Nafion (5% w/w in water and 1-propanol). The mixture was sonicated for 2 hours and then dispersed evenly on piranha-etched glass. The films were dried in the air.

Femtosecond Transient Optical Absorption Spectroscopy (fs-OTA). The fs-OTA spectroscopy is based on a regenerative amplified Ti-Sapphire laser system (Solstice, 800nm, < 100 fs FWHM, 3.5 mJ/pulse, 1 KHz repetition rate). The tunable pump (235-1100nm), chopped at 500Hz, is generated in TOPAS from 75% of the split output from the Ti-Sapphire laser. The other 25% generated tunable UV-visible probe pulses by while light generation in a CaF_2 window (330-720 nm) on a translation stage. Helios ultrafast spectrometer (Ultrafast Systems LLC) was used to collect the spectra. The power of the pump pulse on the sample is 0.25 mW/pulse. The film samples were continuously translated to avoid heating and permanent degradation.

Steady State X-ray Absorption (XAS) spectroscopy. XAS spectra were measured at the beamline 12BM-B at the Advanced Photon Source (APS) in Argonne National Laboratory. The XAS spectra were collected under room temperature with fluorescence mode. The detector was based on 13-element germanium. One ion chamber is placed before the sample and used as the incident X-ray flux reference signal. There are two ion chambers (second and third chambers) after the sample. The Pt foil is placed between the second and third ion chambers and used for energy calibration and collecting Pt metal spectrum. The solid samples were dispersed on Kapton tape for XAS measurement.

X-ray transient absorption (XTA) spectroscopy. XTA spectroscopy was performed at the beamline 11ID-D, APS, Argonne National Laboratory. Samples are prepared by mixing 30mg MOF in 70 mL ACN, sonicate for 30mins.The laser pump was based on a Nd:YLF regenerative amplified laser (1054nm, 1.6 kHz repetition rate, 5 ps FWHM). The pump wavelength at 490 nm was obtained from second harmonic generation output. The laser pump and X-ray probe intersect at a flowing sample stream with 550 μm in diameter. The X-ray fluorescence signals were collected at 90˚ angle on both sides of the incident X-ray beam by two avalanche photodiodes(APDs). A soller slits/Zn filter combination, which was custom designed for the specific sample chamber configuration and the distance between the sample and the detector, was inserted between the sample stream and the APD detectors. The emitted Pt X-ray fluorescence collected at 300ps after the laser pump pulse excitation was used to build the laser-on spectrum in advanced photon source hybrid mode.

Photocatalytic hydrogen evolution reaction for Ru-Pt-UIO-67. Samples for photocatalytic hydrogen production were prepared in 11 mL septum-sealed glass vials. Each sample was made up to a volume of 4 mL, including 0.5 mg of MOF, 3 mL of CH_3CN, and 0.3 mL of H_2O. 0.3 mL of DMA (N, N-dimethylaniline) was added and used as the sacrificial reducing agent. The mixture was purged with N_2 for 15 min before irradiation by a 420 nm cut off Xe lamp (150 w). The mixture was kept stirring during photocatalytic reaction. The amount of H_2 generated was quantified using Agilent 490 micro gas chromatograph (5 Å molecular sieve column) by analyzing 200 μL headspace.

Results and Discussion.

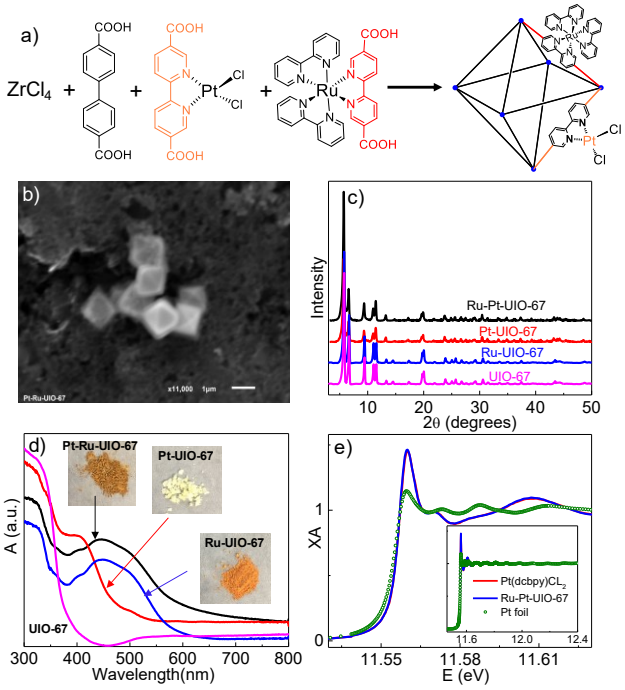

Figure 1. Synthetic scheme (a) and SEM image of Ru-Pt-UIO-67 MOF. XRD patterns (c) and reflectance UV-visible spectra (d) of Ru-Pt-UIO-67, Pt-UIO-67, Ru-UIO-67 and UIO-67. (e) XANES spectra of Ru-Pt-UIO-67, Pt(dcbpy)Cl_2 and Pt foil at Pt L_3-edge. The inset shows their EXAFS spectra.

Ru-Pt-UIO-67 as well as control samples including Pt-UIO-67, Ru-UIO-67, and UIO-67 were synthesized according to previously published literature protocols.[43, 58] The morphology of these MOF samples were examined by SEM. As shown in Figure 1b, Ru-Pt-UIO-67 MOF particle show octahedral or quasi-octahedral shape with sizes ranging from 500-1000 nm, which are similar to the morphology of Pt-UIO-67 and Ru-UIO-67 MOF particles (Figure S1). The surface area and pore size of Ru-Pt-UIO-67 are 1504 m^2/g and 1.65 nm (Figure S1), respectively, which are comparable to literature data,[40, 59] suggesting the porous structure of Ru-Pt-UIO-67 MOF. Figure 1c shows the XRD patterns of the above four MOFs. All of the peaks that correspond to UIO-67 occur in Pt or/and Ru incorporated MOFs, suggesting the retention of parent framework after incorporating molecular moieties. The incorporation of Ru and Pt moieties was confirmed by diffuse reflectance UV-visible spectroscopy. As shown in Figure 1d, compared to the absorption spectrum of UIO-67, an additional broad band (~ 400-600 nm) was observed in the spectrum of

Ru-Pt-UIO-67. This broad band is consistent with the combined absorption of Pt complex in Pt-UIO-67 and Ru complexes in Ru-UIO-67, and thus can be attributed to the absorption resulting from Pt and Ru moieties incorporated into UIO-67. EDX analysis in random areas suggested that Zr, Ru, Pt elements were abundantly distributed in Ru-Pt-UIO-67 with elemental ratio of Ru/Pt about 1.4 (Figure S2).

In addition to the bulk structure, the local coordination environment of Pt center was examined by steady-state X-ray absorption spectroscopy (XAS). Figure 1e shows the X-ray absorption near edge structure (XANES) spectra of Ru-Pt-UIO-67 collected at Pt L_3-edge. For comparison, the XANES spectra of Pt foil and molecular Pt(dcbpy)Cl_2[60] complex were also shown in Figure 1e as reference spectra. As shown in Figure 1e, the white line intensity of Ru-Pt-UIO-67 at 11.568 keV, corresponding to $2p_{2/3}$ to 5d transition, is significantly higher that of Pt foil while remains similar to that of Pt(dcbpy)Cl_2 sample. As the white line intensity of Pt center is directly related to its density of unoccupied d states,[61-62] the similar amplitude of this transition among Ru-Pt-UIO-67 MOF and Pt(dcbpy)Cl_2 complex, which is much larger than that of Pt foil, suggests that Pt-moiety incorporated into MOF structure retains its Pt^{II} oxidation state as that in molecular Pt(dcbpy)Cl_2. To gain insight on the local coordination structure of Pt in MOF samples, we quantitatively analyzed the extended X-ray absorption fine structure (EXAFS) spectra of these samples using FEFF model (Figure S3). The resulting fitting parameters are listed in Table S1. It is found that the coordination numbers and bond distances of Pt to N atoms in dcbpy and Pt to Cl atoms remain same among both samples, further supporting that the structure of Pt(dcbpy)Cl_2 retains during MOF synthesis.

The photocatalytic performance of Ru-Pt-UIO-67 MOF for light-driven H_2 generation was examined under illumination of a broad band Xe lamp, where the IR and UV light from the Xe

lamp was extensively filterd by water filter and 420 nm long-pass filter, respectively. The

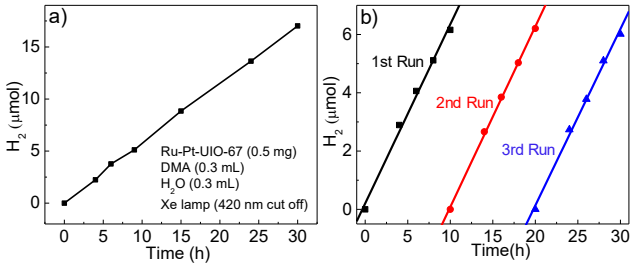

Figure 2. (a) Time profile of H_2 production by Ru-Pt-UIO-67 under Xe lamp illumination in the presence of DMA (0.3 mL) and H_2O (0.3 mL) in acetonitrile solution (3 mL). (b) Recycling of Ru-Pt-UIO-67 catalyst after multiple 10-hour experiments.

experimental parameters such as the sacrificial donors, solvents, and the amount of proton source and MOF particles were systematically varied to find out the conditions that can generate the maximum amount of H_2 per gram of catalyst (Figure S4). Based on these experiments, the optimized condition for the Ru-Pt-UIO-67 photocatalytic system is under Pt-Ru-UIO-67 (0.5 mg), 0.3 mL of H_2O, and 0.3 mL of DMA (N, N-dimethylaniline) in 3 mL acetonitrile solution. Control experiments in the absence of either DMA or H_2O do not produce H_2 (Figure S5), suggesting their key roles as sacrificial donor and proton source, respectively. The systems using Pt-UIO-67 or Ru-UIO-67 with the same metal loading as that in Ru-Pt-UIO-67 produce negligible amount of H_2 (Figure S4), suggesting that both Ru- and Pt-moiety are essential for H_2 generation. Shown in Figure 2a is the full time profile of H_2 generation collected under the optimum condition. The system produces H_2 steadily for at least 30 hours, achieving 34,000 μmol H_2/g of MOF, corresponding to TON of 801 in terms of Pt. As shown in our optimization experiments (Table S2), the performance of Ru-Pt-UIO-67 for H_2 generation can be easily affected by a number of experimental parameters, we attributed the significantly enhanced H_2 activity and elongated duration in current system with respect to the previous result[40] to the difference of the catalytic conditions, suggesting the necessity of performing optimization experiments carefully.

To gain insight into the recyclability of the system, we stopped the reaction every 10 hours and collected Ru-Pt-UIO MOFs from the reaction mixture via centrifugation. The resulting Ru-Pt-UIO-67 MOFs were washed with acetonitrile and redispersed in a fresh catalysis mixture for H_2 generation experiment. As shown in Figure 2b, the catalytic activity of the system does not

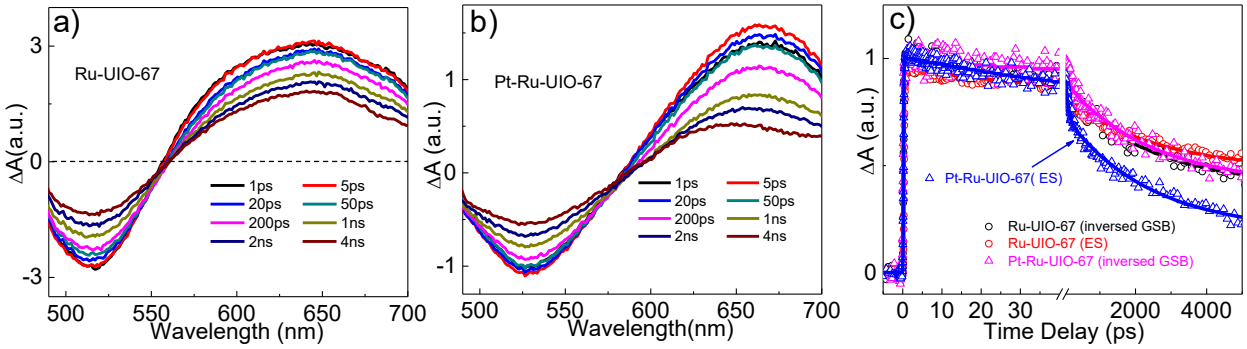

Figure 3. Femtosecond OTA spectra of Ru-UIO-67 (a) and Ru-Pt-UIO-67 (b). (c) The comparisons of the ground state bleach (GSB) recovery and excited state decay kinetics between Ru-UIO-67 and Ru-Pt-UIO-67. The GSB recovery kinetics for both Ru-UIO-67 and Ru-Pt-UIO-67 were inverted for better comparison.

decrease at least 3 cycles of experiments, suggesting that Ru-Pt-UIO-67 MOF catalysts are recyclable.

While the photocatalytic experiments above successfully demonstrate the capability of Ru-Pt-UIO-67 MOF as efficient and robust photocatalysts for H_2 generation and both Ru- and Pt- moiety play important roles in catalysis, it is essential to examine the CS dynamics to unravel the specific roles these moieties play in catalysis. The CS dynamics in Ru-Pt-UIO-67 MOF was examined using optical transient absorption (OTA) spectroscopy. Due to the spectral overlap between Ru- and Pt-moiety in the UV-visible region (Figure 1d), 480 nm pump light was used as excitation source such that majority of the excitation light was absorbed by Ru-moiety. Indeed, the direct excitation of Pt-UIO-67 MOFs yields negligible OTA signals, we can thus exclude the contribution of Pt-moiety to the OTA signals in the spectra of Ru-Pt-UIO-67 due to direct excitation of Pt-moiety. Figure 3a and 3b show the femtosecond OTA spectra of Ru-UIO-67 and Ru-Pt-UIO-67,

respectively. The OTA spectra of Ru-UIO-67 were used as control to illustrate the intrinsic excited state (ES) dynamics of Ru-moiety in MOF framework in the absence of Pt-moiety. As shown in Figure 3a, the OTA spectra of Ru-UIO-67 consist of a negative band centered at ~ 514 nm and a broad absorption band at ~ 634 nm, which can be attributed to the ground state bleach (GSB) and ES absorption of Ru-moiety, respectively. The recovery of GSB and decay of ES follow the same kinetics (Figure 3c), as well as the presence of a clear isosbestic point at 554 nm between these two spectral features, suggesting that the recovery/decay kinetics of these two species represent the same recombination process, i.e. the intrinsic recovery of GS molecules from ES. While the similar GSB and ES absorption were observed in the OTA spectra of Ru-Pt-UIO-67, distinct differences were observed between two spectra. As shown in Figure 3c, while the GSB recovery kinetics of Ru-Pt-UIO-67 remains similar to that of Ru-UIO-67, the ES absorption in Ru-Pt-UIO-67 decays much faster than that in Ru-UIO-67. These results are consistent with the spectral features when electron transfer (ET) process occurs, suggesting that ET from Ru- to Pt-moiety in Ru-Pt-UIO-67 is responsible for the enhanced ES decay in Ru-Pt-UIO-67 MOF. As shown in Table S3, the GSB recovery and ES decay kinetic traces of Ru-UIO-67 as well as GSB recovery of Ru-Pt-UIO-67 can all be fit by the same three-exponential decay function. The ES decay kinetic trace of Ru-moiety in Ru-Pt-UIO-67 can also be fit by a three-exponential decay function. However, due to the presence of a long-lived decay component (>> 5 ns) which is beyond our OTA time window, we are not able to accurately determine the ET time from the fitting results. Instead, we compared the half lifetime of ES decay dynamics of Ru-moiety in both samples, which is 4.9 ns and 1.2 ns for Ru-UIO-67 and Ru-Pt-UIO-67, respectively. The much shorter half lifetime of Ru-moiety ES in Ru-Pt-UIO-67 than Ru-UIO-67 suggests that ET occurs from excited Ru- to Pt-moiety. Moreover, the half lifetime of GSB of Ru-moiety in Ru-Pt-UIO-67 (~4.9 ns) is longer

than its ES decay, suggesting that the charge recombination process between the reduced Pt-moiety and the oxidized Ru-moiety is slower than ET process.

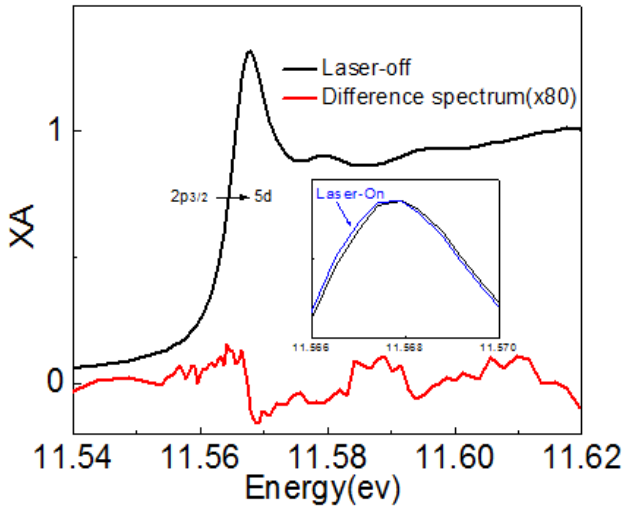

Figure 4. XANES spectrum of Ru-Pt-UIO-67 at Pt L_3-edge (black plot). The difference XANES spectrum (red plot), obtained by subtracting the laser-off spectrum from laser-on spectrum (300 ps after excitation), is also shown in the figure. Inset shows enlarged laser-on and laser-off spectrum

The formation of the charge separated state in Ru-Pt-UIO-67 MOF due to ET from Ru- to Pt-moiety was further supported by probing the photoinduced electron density change at Pt center following the excitation of Ru-moiety using X-ray transient absorption (XTA) spectroscopy. Figure 4 shows the Pt L_3-edge XANES spectra of Ru-Pt-UIO-67 before (laser-off spectrum, black plot) and 300 ps (laser-on spectrum, not shown) after 480 nm excitation. The transient signal due to laser excitation was clearly observed in the difference spectrum (red plot) obtained after subtracting the laser-off spectrum from the laser-on spectrum. The positive feature at 11.565 keV where $2p_{2/3}$ to 5d transition occurs indicates that the edge of Pt center shifts to lower energy, supporting the formation of reduced Pt center. The reduction of Pt center due to photoexcitation of Ru-moiety is further confirmed by the negative signal at 11.568 keV which corresponds to the

reduced intensity of the white line amplitude, i.e. decreased oxidation state of Pt due to photoexcitation. As shown in Figure S6, similar difference shows up at different delay times while no difference was observed for Pt-UIO-67 control sample. These results unambiguously confirm the ET process from excited Ru- to Pt-moiety, consistent with OTA results above.

Conclusion.

In summary, we have synthesized a hybrid Zr-MOF with simultaneously incorporated molecular Ru-photosensitizer and Pt-catalyst, which is highly active, robust, and recyclable for catalyzing proton reduction to generate H_2 reaction. Using the combination of advanced ultrafast OTA and XTA spectroscopy, we investigated the CS dynamics in this hybrid MOF. We show that CS in Ru-Pt-UIO-67 MOF occurs through ET from excited Ru- to Pt-moiety, which unambiguously unraveled the fundamental roles of the incorporated homogeneous components in the heterogeneous MOF matrix for photocatalytic reaction, providing important guidance in rational design of hybrid MOF systems for solar to fuel conversion.

ASSOCIATED CONTENT

Supporting Information. The details of sample synthesis, standard characterization, XAS experiments, OTA experiment, XTA experiment, the SEM images, EDX results, the fitting results of XAS and OTA, and the optimization for photocatalytic conditions are available free of charge via the Internet at http://pubs.acs.org."

AUTHOR INFORMATION

*Jier Huang (jier.huang@marquette.edu)

The authors declare no competing financial interests.

ACKNOWLEDGMENT

This work was supported by National Science Foundation (DMR-1654140) and ACS-PRF (57503-DNI6). Use of the Advanced Photon Source in Argonne National Laboratory was supported by the U. S. Department of Energy, Office of Science, Office of Basic Energy Sciences, under Award No. DE-AC02-06CH11357. We thank the help from Xin Zhang and Dr. Jian Zhang in University of Nebraska-Lincoln for BET measurements.

REFERENCES

1. Gratzel, M. Artificial Photosynthesis - Water Cleavage into Hydrogen and Oxygen by Visible-Light. *Acc. Chem. Res.* **1981**, *14*, 376-384.

2. Chen, X. B.; Shen, S. H.; Guo, L. J.; Mao, S. S. Semiconductor-Based Photocatalytic Hydrogen Generation. *Chem. Rev.* **2010**, *110*, 6503-6570.

3. Wen, F. Y.; Li, C. Hybrid Artificial Photosynthetic Systems Comprising Semiconductors as Light Harvesters and Biomimetic Complexes as Molecular Cocatalysts. *Acc. Chem. Res.* **2013**, *46*, 2355-2364.

4. Bard, A. J.; Fox, M. A. Artificial Photosynthesis - Solar Splitting of Water to Hydrogen and Oxygen. *Acc. Chem. Res.* **1995**, *28*, 141-145.

5. Han, Z. J.; Qiu, F.; Eisenberg, R.; Holland, P. L.; Krauss, T. D. Robust Photogeneration of H_2 in Water Using Semiconductor Nanocrystals and a Nickel Catalyst. *Science* **2012**, *338*, 1321-1324.

6. Das, A.; Han, Z. J.; Haghighi, M. G.; Eisenberg, R. Photogeneration of Hydrogen from Water Using Cdse Nanocrystals Demonstrating the Importance of Surface Exchange. *Proc. Natl. Acad. Sci.* **2013**, *110*, 16716-16723.

7. McNamara, W. R.; Han, Z. J.; Alperin, P. J.; Brennessel, W. W.; Holland, P. L.; Eisenberg, R. A Cobalt-Dithiolene Complex for the Photocatalytic and Electrocatalytic Reduction of Protons. *J. Am. Chem. Soc.* **2011**, *133*, 15368-15371.

8. Gartner, F.; Sundararaju, B.; Surkus, A. E.; Boddien, A.; Loges, B.; Junge, H.; Dixneuf, P. H.; Beller, M. Light-Driven Hydrogen Generation: Efficient Iron-Based Water Reduction Catalysts. *Angew. Chem., Int. Ed.* **2009**, *48*, 9962-9965.

9. Han, Z. J.; McNamara, W. R.; Eum, M. S.; Holland, P. L.; Eisenberg, R. A Nickel Thiolate Catalyst for the Long-Lived Photocatalytic Production of Hydrogen in a Noble-Metal-Free System. *Angew. Chem., Int, Ed.* **2012**, *51*, 1667-1670.

10. Fihri, A.; Artero, V.; Pereira, A.; Fontecave, M. Efficient H_2-Producing Photocatalytic Systems Based on Cyclometalated Iridium- and Tricarbonylrhenium-Diimine Photosensitizers and Cobaloxime Catalysts. *Dalton Trans.* **2008**, 5567-5569.

11. Sakata, T.; Kawai, T.; Hashimoto, K. Photochemical Diode Model of Pt-TiO_2 Particle and Its Photocatalytic Activity. *Chem. Phys. Lett.* **1982**, *88*, 50-54.

12. Acharya, K. P.; Khnayzer, R. S.; O'Connor, T.; Diederich, G.; Kirsanova, M.; Klinkova, A.; Roth, D.; Kinder, E.; Imboden, M.; Zamkov, M. The Role of Hole Localization in Sacrificial

Hydrogen Production by Semiconductor-Metal Heterostructured Nanocrystals. *Nano Lett.* **2011**, *11*, 2919-2926.

13. Berr, M.; Vaneski, A.; Susha, A. S.; Rodriguez-Fernandez, J.; Doblinger, M.; Jackel, F.; Rogach, A. L.; Feldmann, J. Colloidal CdS Nanorods Decorated with Subnanometer Sized Pt Clusters for Photocatalytic Hydrogen Generation. *Appl. Phys. Lett.* **2010**, *97*.

14. Amirav, L.; Alivisatos, A. P. Photocatalytic Hydrogen Production with Tunable Nanorod Heterostructures. *J. Phys. Chem. Lett.* **2010**, *1*, 1051-1054.

15. Yan, H. J.; Yang, J. H.; Ma, G. J.; Wu, G. P.; Zong, X.; Lei, Z. B.; Shi, J. Y.; Li, C. Visible-Light-Driven Hydrogen Production with Extremely High Quantum Efficiency on Pt-PdS/CdS Photocatalyst. *J. Catal.* **2009**, *266*, 165-168.

16. Rosi, N. L.; Eckert, J.; Eddaoudi, M.; Vodak, D. T.; Kim, J.; O'Keeffe, M.; Yaghi, O. M. Hydrogen Storage in Microporous Metal-Organic Frameworks. *Science* **2003**, *300*, 1127-1129.

17. Zhou, H. C.; Long, J. R.; Yaghi, O. M. Introduction to Metal-Organic Frameworks. *Chem. Rev.* **2012**, *112*, 673-674.

18. Cook, T. R.; Zheng, Y. R.; Stang, P. J. Metal-Organic Frameworks and Self-Assembled Supramolecular Coordination Complexes: Comparing and Contrasting the Design, Synthesis, and Functionality of Metal-Organic Materials. *Chem. Rev.* **2013**, *113*, 734-777.

19. Wang, C.; Liu, D. M.; Lin, W. B. Metal-Organic Frameworks as a Tunable Platform for Designing Functional Molecular Materials. *J. Am. Chem. Soc.* **2013**, *135*, 13222-13234.

20. Kitagawa, S.; Kitaura, R.; Noro, S. Functional Porous Coordination Polymers. *Angew. Chem., Int. Ed.* **2004**, *43*, 2334-2375.

21. Moulton, B.; Zaworotko, M. J. From Molecules to Crystal Engineering: Supramolecular Isomerism and Polymorphism in Network Solids. *Chem. Rev.* **2001**, *101*, 1629-1658.

22. Farha, O. K.; Spokoyny, A. M.; Mulfort, K. L.; Hawthorne, M. F.; Mirkin, C. A.; Hupp, J. T. Synthesis and Hydrogen Sorption Properties of Carborane Based Metal-Organic Framework Materials. *J. Am. Chem. Soc.* **2007**, *129*, 12680-+.

23. Foo, M. L.; Matsuda, R.; Kitagawa, S. Functional Hybrid Porous Coordination Polymers. *Chem. Mater.* **2014**, *26*, 310-322.

24. Li, Z.; Xiao, J. D.; Jiang, H. L. Encapsulating a Co(II) Molecular Photocatalyst in Metal-Organic Framework for Visible-Light-Driven H_2 Production: Boosting Catalytic Efficiency Via Spatial Charge Separation. *ACS Catal.* **2016**, *6*, 5359-5365.

25. Chambers, M. B.; Wang, X.; Elgrishi, N.; hendon, C. H.; Walsh, A.; Bonnefoy, J.; Canivet, J.; Auadrelli, E. A.; Farrusseng, D.; Mellot-Draznieks, C. et al. Photocatalytic Carbon Dioxide Reduction with Rhodium-Based Catalysts in Solution and Heterogenized within Metal-Organic Frameworks. *ChemSusChem* **2015**, *8*, 603-608.

26. Zhang, T.; Manna, K.; Lin, W. B. Metal-Organic Frameworks Stabilize Solution-Inaccessible Cobalt Catalysts for Highly Efficient Broad-Scope Organic Transformations. *J. Am. Chem. Soc.* **2016**, *138*, 3241-3249.

27. Rimoldi, M.; Nakamura, A.; Vermeulen, N. A.; Henkelis, J. J.; Blackburn, A. K.; Hupp, J. T.; Stoddart, J. F.; Farha, O. K. A Metal-Organic Framework Immobilised Iridium Pincer Complex. *Chem. Sci.* **2016**, *7*, 4980-4984.

28. Kim, D.; Whang, D. R.; Park, S. Y. Self-Healing of Molecular Catalyst and Photosensitizer on Metal-Organic Framework: Robust Molecular System for Photocatalytic H_2 Evolution from Water. *J. Am. Chem. Soc.* **2016**, *138*, 8698-701.

29. de Miguel, M.; Ragon, F.; Devic, T.; Serre, C.; Horcajada, P.; Garcia, H. Evidence of Photoinduced Charge Separation in the Metal-Organic Framework Mil-125(Ti)-Nh_2. *ChemPhysChem* **2012**, *13*, 3651-4.

30. Laurier, K. G.; Fron, E.; Atienzar, P.; Kennes, K.; Garcia, H.; Van der Auweraer, M.; De Vos, D. E.; Hofkens, J.; Roeffaers, M. B. Delayed Electron-Hole Pair Recombination in Iron(III)-Oxo Metal-Organic Frameworks. *Phys. Chem. Chem. Phys.* **2014**, *16*, 5044-7.

31. Fateeva, A.; Chater, P. A.; Ireland, C. P.; Tahir, A. A.; Khimyak, Y. Z.; Wiper, P. V.; Darwent, J. R.; Rosseinsky, M. J. A Water-Stable Porphyrin-Based Metal-Organic Framework Active for Visible-Light Photocatalysis. *Angew. Chem., Int. Ed.* **2012**, *51*, 7440-7444.

32. Takaishi, S.; DeMarco, E. J.; Pellin, M. J.; Farha, O. K.; Hupp, J. T. Solvent-Assisted Linker Exchange (Sale) and Post-Assembly Metallation in Porphyrinic Metal-Organic Framework Materials. *Chem. Sci.* **2013**, *4*, 1509-1513.

33. Barron, P. M.; Wray, C. A.; Hu, C. H.; Guo, Z. Y.; Choe, W. A Bioinspired Synthetic Approach for Building Metal-Organic Frameworks with Accessible Metal Centers. *Inorg. Chem.* **2010**, *49*, 10217-10219.

34. Lee, C. Y.; Farha, O. K.; Hong, B. J.; Sarjeant, A. A.; Nguyen, S. T.; Hupp, J. T. Light-Harvesting Metal-Organic Frameworks (MOFs): Efficient Strut-to-Strut Energy Transfer in Bodipy and Porphyrin-Based MOFs. *J. Am. Chem. Soc.* **2011**, *133*, 15858-15861.

35. Xu, H. Q.; Hu, J. H.; Wang, D. K.; Li, Z. H.; Zhang, Q.; Luo, Y.; Yu, S. H.; Jiang, H. L. Visible-Light Photoreduction of CO_2 in a Metal-Organic Framework: Boosting Electron-Hole Separation Via Electron Trap States. *J. Am. Chem. Soc.* **2015**, *137*, 13440-13443.

36. Fateeva, A.; Chater, P. A.; Ireland, C. P.; Tahir, A. A.; Khimyak, Y. Z.; Wiper, P. V.; Darwent, J. R.; Rosseinsky, M. J. A Water-Stable Porphyrin-Based Metal-Organic Framework Active for Visible-Light Photocatalysis. *Angew. Chem., Int. Ed.* **2012**, *51*, 7440-7444.

37. Kent, C. A.; Mehl, B. P.; Ma, L. Q.; Papanikolas, J. M.; Meyer, T. J.; Lin, W. B. Energy Transfer Dynamics in Metal-Organic Frameworks. *J. Am. Chem. Soc.* **2010**, *132*, 12767-12769.

38. Maza, W. A.; Padilla, R.; Morris, A. J. Concentration Dependent Dimensionality of Resonance Energy Transfer in a Postsynthetically Doped Morphologically Homologous Analogue of UIO-67 Mof with a Ruthenium(II) Polypyridyl Complex. *J. Am. Chem. Soc.* **2015**, *137*, 8161-8168.

39. Zhang, S. Q.; Li, L. N.; Zhao, S. G.; Sun, Z. H.; Luo, J. H. Construction of Interpenetrated Ruthenium Metal-Organic Frameworks as Stable Photocatalysts for CO_2 Reduction. *Inorg. Chem.* **2015**, *54*, 8375-8379.

40. Hou, C. C.; Li, T. T.; Cao, S.; Chen, Y.; Fu, W. F. Incorporation of a $[Ru(Dcbpy)(Bpy)_2]^{2+}$ Photosensitizer and a $Pt(Dcbpy)Cl_2$ Catalyst into Metal-Organic Frameworks for Photocatalytic Hydrogen Evolution from Aqueous Solution. *J. Mater. Chem. A* **2015**, *3*, 10386-10394.

41. Wei, Z. W.; Gu, Z. Y.; Arvapally, R. K.; Chen, Y. P.; McDougald, R. N.; Ivy, J. F.; Yakovenko, A. A.; Feng, D. W.; Omary, M. A.; Zhou, H. C. Rigidifying Fluorescent Linkers by Metal-Organic Framework Formation for Fluorescence Blue Shift and Quantum Yield Enhancement. *J. Am. Chem. Soc.* **2014**, *136*, 8269-8276.

42. Kataoka, Y.; Sato, K.; Miyazaki, Y.; Masuda, K.; Tanaka, H.; Naito, S.; Mori, W. Photocatalytic Hydrogen Production from Water Using Porous Material $[Ru_2(P\text{-}BDC)_2]_n$. *Energy Environ. Sci.* **2009**, *2*, 397-400.

43. Wang, C.; Xie, Z. G.; deKrafft, K. E.; Lin, W. L. Doping Metal-Organic Frameworks for Water Oxidation, Carbon Dioxide Reduction, and Organic Photocatalysis. *J. Am. Chem. Soc.* **2011**, *133*, 13445-13454.

44. Huang, R. Y.; Peng, Y.; Wang, C.; Shi, Z.; Lin, W. B. A Rhenium-Functionalized Metal-Organic Framework as a Single-Site Catalyst for Photochemical Reduction of Carbon Dioxide. *Eur. J. Inorg. Chem.* **2016**, 4358-4362.

45. Nasalevich, M. A.; Becker, R.; Ramos-Fernandez, E. V.; Castellanos, S.; Veber, S. L.; Fedin, M. V.; Kapteijn, F.; Reek, J. N. H.; van der Vlugt, J. I.; Gascon, J. Co@NH_2-MIL-125(Ti): Cobaloxime-Derived Metal-Organic Framework-Based Composite for Light-Driven H_2 Production. *Energy Environ. Sci.* **2015**, *8*, 364-375.

46. Sasan, K.; Lin, Q. P.; Mao, C. Y.; Feng, P. Y. Incorporation of Iron Hydrogenase Active Sites into a Highly Stable Metal-Organic Framework for Photocatalytic Hydrogen Generation. *Chem. Commun.* **2014**, *50*, 10390-10393.

47. Pullen, S.; Fei, H. H.; Orthaber, A.; Cohen, S. M.; Ott, S. Enhanced Photochemical Hydrogen Production by a Molecular Diiron Catalyst Incorporated into a Metal-Organic Framework. *J. Am. Chem. Soc.* **2013**, *135*, 16997-17003.

48. Kim, D.; Whang, D. R.; Park, S. Y. Self-Healing of Molecular Catalyst and Photosensitizer on Metal-Organic Framework: Robust Molecular System for Photocatalytic H_2 Evolution from Water. *J. Am. Chem. Soc.* **2016**, *138*, 8698-8701.

49. Zhou, T. H.; Du, Y. H.; Borgna, A.; Hong, J. D.; Wang, Y. B.; Han, J. Y.; Zhang, W.; Xu, R. Postc-Synthesis Modification of a Metalc-Organic Framework to Construct a Bifunctional Photocatalyst for Hydrogen Production. *Energy Environ. Sci.* **2013**, *6*, 3229-3234.

50. Kim, D.; Whang, D. R.; Park, S. Y. Self-Healing of Molecular Catalyst and Photosensitizer on Metal–Organic Framework: Robust Molecular System for Photocatalytic H2 Evolution from Water. *J. Am. Chem. Soc.* **2016**, *138*, 8698-8701.

51. Maza, W. A.; Morris, A. J. Photophysical Characterization of a Ruthenium(II) Tris(2,2 ' Bipyridine)-Doped Zirconium UIO-67 Metal Organic Framework. *J. Phys. Chem. C* **2014**, *118*, 8803-8817.

52. Roy, S.; Pascanu, V.; Pullen, S.; Miera, G. G.; Martin-Matute, B.; Ott, S. Catalyst Accessibility to Chemical Reductants in Metal-Organic Frameworks. *Chem. Commun.* **2017**, *53*, 3257-3260.

53. So, M. C.; Wiederrecht, G. P.; Mondloch, J. E.; Hupp, J. T.; Farha, O. K. Metal-Organic Framework Materials for Light-Harvesting and Energy Transfer. *Chem. Commun.* **2015**, *51*, 3501-3510.

54. Kent, C. A.; Liu, D. M.; Ma, L. Q.; Papanikolas, J. M.; Meyer, T. J.; Lin, W. B. Light Harvesting in Microscale Metal-Organic Frameworks by Energy Migration and Interfacial Electron Transfer Quenching. *J. Am. Chem. Soc.* **2011**, *133*, 12940-12943.

55. Kent, C. A.; Liu, D.; Meyer, T. J.; Lin, W. Amplified Luminescence Quenching of Phosphorescent Metal-Organic Frameworks. *J. Am. Chem. Soc.* **2012**, *134*, 3991-3994.

56. Atkins, M. J.; Harwood, D. J.; Lowry, R. B. Synthesis and Characterisation of a Novel Ruthenium Organometallic cis-$Ru(Bpy)_2(npp)(Cl)\cdot BF_4$ Where bpy=2,2'-Bipyridyl and npp=4-(N-Pyrrolyl)Pyridine. *Inorg. Chim. Acta* **1996**, *244*, 277-280.

57. Price, J. H.; Schramm, R. F.; Wayland, B. B.; Williamson, A. N. Palladium(II) and Platinum(II) Alkyl Sulfoxide Complexes - Examples of Sulfur-Bonded, Mixed Sulfur-Bonded and Oxygen-Bonded, and Totally Oxygen-Bonded Complexes. *Inorg. Chem.* **1972**, *11*, 1280-+.

58. Pullen, S.; Fei, H.; Orthaber, A.; Cohen, S. M.; Ott, S. Enhanced Photochemical Hydrogen Production by a Molecular Diiron Catalyst Incorporated into a Metal–Organic Framework. *J. Am. Chem. Soc.* **2013**, *135*, 16997-17003.

59. Wang, C.; deKrafft, K. E.; Lin, W. B. Pt Nanoparticles@Photoactive Metal-Organic Frameworks: Efficient Hydrogen Evolution Via Synergistic Photoexcitation and Electron Injection. *J. Am. Chem. Soc.* **2012**, *134*, 7211-7214.

60. Canty, A. J.; Gardiner, M. G.; Jones, R. C.; Sharma, M. Structural Chemistry of MX_2(bipy) (M = Pd, Pt; X = Cl, Br, I): The Yellow Polymorph of Dichlorido(2,2 '-Bipyridine)Platinum(II) and Diiodido(2,2 '-Bipyridine)Palladium(II), and Overview of This System. *Aust. J. Chem.* **2011**, *64*, 1355-1359.

61. Tsai, Y. W.; Tseng, Y. L.; Sarma, L. S.; Liu, D. G.; Lee, J. F.; Hwang, B. J. Genesis of Pt Clusters in Reverse Micelles Investigated by in Situ X-Ray Absorption Spectroscopy. *J. Phys. Chem. B* **2004**, *108*, 8148-8152.

62. Horsley, J. A. Relationship between the Area of $L_{2,3}$ X-Ray Absorption-Edge Resonances and the D Orbital Occupancy in Compounds of Platinum and Iridium. *J. Chem. Phys.* **1982**, *76*, 1451-1458.

TOC Graphic